Mon. Not. R. Astron. Soc. **000**, 1–16 (20XX) Printed 2 December 2009 (MN LATEX style file v2.2)

Observational constraints on an interacting dark energy model

Jussi Väliviita,[1] Roy Maartens[1] and Elisabetta Majerotto[2,1]
[1] *Institute of Cosmology & Gravitation, University of Portsmouth, Portsmouth PO1 3FX, United Kingdom*
[2] *INAF-Osservatorio Astronomico di Brera, Via Bianchi 46, I-23807 Merate (LC), Italy*

Accepted 2009 November 25. Received 2009 November 17; in original form 2009 September 19

ABSTRACT

We use observations of cosmic microwave background anisotropies, supernova luminosities and the baryon acoustic oscillation signal in the galaxy distribution to constrain the cosmological parameters in a simple interacting dark energy model with a time-varying equation of state. Using a Monte Carlo Markov Chain technique we determine the posterior likelihoods. Constraints from the individual data sets are weak, but the combination of the three data sets confines the interaction constant Γ to be less than 23% of the expansion rate of the Universe H_0; at 95% CL $-0.23 < \Gamma/H_0 < +0.15$. The CMB acoustic peaks can be well fitted even if the interaction rate is much larger, but this requires a larger or smaller (depending on the sign of interaction) matter density today than in the non-interacting model. Due to this degeneracy between the matter density and the interaction rate, the only observable effect on the CMB is a larger or smaller integrated Sachs–Wolfe effect. While SN or BAO data alone do not set any direct constraints on the interaction, they exclude the models with very large matter density, and hence indirectly constrain the interaction rate when jointly analysed with the CMB data. To enable the analysis described in this paper, we present in a companion paper [arXiv:0907.4981] a new systematic analysis of the early radiation era solution to find the adiabatic initial conditions for the Boltzmann integration.

Key words: cosmology:theory, cosmology:observations, cosmic microwave background, cosmological parameters, dark matter, large-scale structure of Universe

1 INTERACTING DARK ENERGY

Dark energy and dark matter are the dominant sources in the 'standard' model for the evolution of the universe. Both are currently only detected via their gravitational effects, with an inevitable degeneracy between them (one requires a model to separate dark energy from dark matter). There could thus be an interaction between them that is consistent with current observational constraints. A dark sector interaction could also alleviate the 'coincidence' problem (why are the energy densities of the two components of the same order of magnitude today?). Furthermore, interacting dark energy exerts a non-gravitational 'drag' on dark matter, and thus can introduce new features to structure formation, including possibly a new large-scale bias (Amendola & Tocchini-Valentini 2002) and a violation by dark matter of the weak equivalence principle on cosmological scales (Bertolami et al. 2007; Koyama et al. 2009).

The energy balance equations in the background are

$$\rho_c' = -3\mathcal{H}\rho_c + aQ_c\,, \quad (1)$$

$$\rho_{de}' = -3\mathcal{H}(1+w_{de})\rho_{de} + aQ_{de}\,, \quad Q_{de} = -Q_c\,, \quad (2)$$

where a is the scale factor of the Universe, $\mathcal{H} = a'/a$ is the conformal Hubble parameter, $w_{de} = p_{de}/\rho_{de}$ is the dark energy equation of state parameter, a prime indicates derivative with respect to conformal time τ, and Q_c is the rate of transfer to the dark matter density due to the interaction.

Various forms for Q_c have been put forward (see, e.g. Wetterich (1995); Amendola (1999); Billyard & Coley (2000); Zimdahl & Pavon (2001); Farrar & Peebles (2004); Chimento et al. (2003); Olivares et al. (2005); Koivisto (2005); Sadjadi & Alimohammadi (2006); Guo et al. (2007); Boehmer et al. (2008); He & Wang (2008); Quartin et al. (2008); Pereira & Jesus (2009); Quercellini et al. (2008); Valiviita et al. (2008); He et al. (2009); Bean et al. (2008); Chongchitnan (2009); Corasaniti (2008); Caldera-Cabral et al. (2009); Gavela et al. (2009); Jackson et al. (2009)). All of these models are phenomenological. Some of them are constructed specifically for mathematical simplicity – for example, models in which $Q_c \propto \mathcal{H}\rho$. Rather than design the interaction to achieve a specific outcome, we prefer to start with a simple physical model, and then develop its predictions.

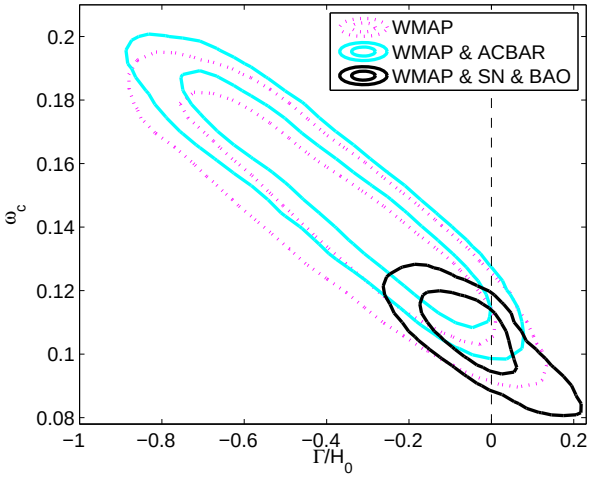

Figure 1. Marginalized likelihoods for the interacting model with WMAP, WMAP&ACBAR, and WMAP&SN&BAO data. The curves show 68% and 95% CL regions: dotted magenta/grey for WMAP, solid cyan/grey for WMAP&ACBAR, and solid black for WMAP&SN&BAO data.

We consider models which are similar to simple models of reheating (Turner 1983), of dark matter decay into radiation (Cen 2001), and of curvaton decay (Malik et al. 2003) – i.e., where the interaction has the form of a decay of one species into another, with constant decay rate. Such a model was introduced in Boehmer et al. (2008); Valiviita et al. (2008):

$$Q_c = -\Gamma\rho_c\,, \tag{3}$$

where Γ is the constant positive decay rate of dark matter to dark energy. Here, as well as in Valiviita et al. (2008), we include also the possibility $\Gamma < 0$, i.e., allow also for energy transfer is from dark energy to dark matter.

In Valiviita, Majerotto & Maartens (2008) we considered the case of fluid dark energy with a *constant* equation of state parameter $-1 < w_{de} \leqslant -4/5$, and found that a serious large-scale non-adiabatic instability affects this model in the early radiation dominated epoch. This instability is stronger the closer w_{de} is to -1. Phantom models, $w_{de} < -1$, do not suffer from this instability, but we consider them to be unphysical.

The instability is determined by the early-time value of w_{de}: for constant w_{de} there is no flexibility, but a *variable* w_{de} (as in quintessence models, see e.g. Lee et al. (2006)) should allow us to avoid the instability. We show that the models are viable if $w_{de} > -4/5$ at early times, while at late times, $w_{de} \sim -1$. We represent w_{de} via the parametrization $w_{de} = w_0 + w_a(1-a)$ (Chevallier & Polarski 2001; Linder 2003), which we rewrite as

$$w_{de} = w_0 a + w_e(1-a)\,, \tag{4}$$

where $w_e = w_0 + w_a$ is the early-time value of w_{de}, while w_0 is the late-time value. This parametrization was originally developed to phenomenologically account for the possible time evolution of w_{de} up to redshifts of a few. At higher redshifts it describes the simplest possible model where w_{de} is a constant, namely w_e. In particular, this parametrization works well for some classes of quintessence models Caldwell & Linder (2005) and it has the advantage of having a finite value at high redshifts. Using a parametrisation for w_{de} has the drawback that it cannot reproduce all possible models for a large redshift range. Furthermore, it is not possible to compute the speed of sound but it is necessary to assume a value for it. It might be interesting to look at different parametrisations of w_{de} or a definite scalar field model. This is left for future work. In this paper we demonstrate with the simple parametrization, Eq. (4), that a (suitably) time-varying w_{de} cures the interacting model, Eq. (3), from the early-time large-scale instability, and thus provides a viable cosmology.

We perform a full Monte Carlo Markov Chain (MCMC) likelihood scan for the spatially flat interacting and non-interacting models, using a modification of the CAMB (Lewis et al. 2000) Boltzmann code, to determine the best-fitting values of Γ/H_0 and the other cosmological parameters, against Wilkinson Microwave Anisotropy Probe (WMAP) 5-years data (Komatsu et al. 2009), Supernovae Ia (SN) Union sample data (Kowalski et al. 2008), and data points for the ratio of the sound horizon to a distance measure at two different redshifts from baryon acoustic oscillation (BAO) observations (Percival et al. 2007). The best-fitting models with various combinations of data are shown in Table A2 on page 14 in Appendix B, while Fig. 1 above summarizes our main findings for the posterior likelihoods. Our most stringent results for the interacting model result from the combined analysis of WMAP&SN&BAO, giving the following minimal 95% intervals: $\omega_b \in (0.0212, 0.0241)$, $\omega_c \in (0.859, 0.125)$, $H_0 \in (63, 70)$, $\tau \in (0.057, 0.133)$, $\Gamma/H_0 \in (-0.23, +0.15)$, $w_e \in (-0.80, -0.19)$, $w_0 \in (-1.00, -0.63)$, $n_S \in (0.937, 1.002)$, $\ln(10^{10}A_S^2) \in (2.95, 3.14)$, $\Omega_{de0} \in (0.648, 0.767)$, Age $\in$ (13.6, 14.3) Gyr. Description and prior ranges of these parameters are given in Appendix A2. There, in Table A1, we also list the definitions of some of the symbols used in this paper.

The key features of the constraints on the interacting model from data may be summarized as follows.

- Any of the data sets alone (CMB, or SN, or BAO) would allow for large interaction: $|\Gamma|$ could be even larger than

Table 1. The evolution of perturbations on super-Hubble scales with various values of the dark energy equation of state parameter in the radiation and matter dominated eras. "Adiabatic" means that it is possible to specify adiabatic initial conditions so that the total gauge invariant curvature perturbation ζ stays constant on super-Hubble scales, and the evolution of all non-dark energy perturbations is the same as in the non-interacting case while the *de* perturbations behave differently. "Adiabatic (standard)" means that the behaviour of all perturbations at early times on super-Hubble scales is the same as in the non-interacting model.

w_{de} in the RD or MD era	Radiation dominated era (RD)	Matter dominated era (MD)	Viable?
$w_{de} < -1$	adiabatic	adiabatic	viable, but phantom
$-1 < w_{de} < -4/5$	"blow-up" isocurvature growth	"blow-up" isocurvature growth	non-viable
$-4/5 \leqslant w_{de} < -2/3$	adiabatic	isocurvature growth	viable, if $\lvert\Gamma\rvert$ small enough
$-2/3 \leqslant w_{de} < -1/2$	adiabatic (standard)	adiabatic	viable
$-1/2 \leqslant w_{de} < +1/3$	adiabatic (standard)	adiabatic (standard)	viable

today's Hubble rate H_0. In the CMB the only hint from a large interaction rate is a modified integrated Sachs–Wolfe (ISW) effect. However, due to the cosmic variance the χ^2 is only mildly affected.

• A large negative Γ fits the CMB TT and TE spectra equally well as the $\Gamma = 0$ model, but a good fit requires a larger physical cold dark matter density today, ω_c, (and hence a smaller Ω_{de0}) and a smaller H_0. Negative Γ suppresses the late ISW effect and hence the CMB fit is slightly better than in the $\Gamma = 0$ case. Combining the CMB data with either SN or BAO or SN&BAO data, this improvement is cancelled by a worse fit to SN and BAO due to too little acceleration at low redshifts.

• Models with large positive Γ fit the high-l CMB TT and all TE data equally well as the $\Gamma = 0$ model, but a good fit requires a smaller ω_c (and hence a larger Ω_{de0}) and a larger H_0. The SN and BAO data can be fitted better than in the $\Gamma = 0$ case due to increased acceleration at small redshifts. However, this improvement is cancelled by a worse fit to the low-l CMB TT spectrum due to a large late ISW effect.

There are two critical features of the analysis of interacting models, which are not always properly accounted for in the literature:

• The background energy transfer rate Q_c does not in itself determine the interaction in the perturbed universe: one must also specify the momentum transfer rate. We do this via a physical assumption, i.e., that the momentum transfer vanishes in the dark matter rest-frame, so that the energy-momentum transfer rate is given covariantly (Valiviita et al. 2008) by

$$Q_c^\mu = Q_c u_c^\mu = -Q_{de}^\mu\,, \quad Q_c = -\Gamma\rho_c(1+\delta_c), \qquad (5)$$

where u_c^μ is the dark matter 4-velocity, and $\delta_c = \delta\rho_c/\rho_c$ is the cold dark matter (CDM) density contrast.

• Adiabatic initial conditions in the presence of a dark sector interaction require a careful analysis of the early-radiation solution. We derive these initial conditions in the companion paper (Majerotto, Valiviita & Maartens 2009) by generalizing the methods of Doran et al. (2003) to the interacting case, extending our previous results (Valiviita et al. 2008). The key results for the initial conditions and early-time perturbation evolution are reproduced in Table 1.

We give here the first analysis of the CMB spectra and the first MCMC likelihood analysis for the interacting model (5), using the perturbation equations and initial conditions given in the companion paper (Majerotto, Valiviita & Maartens 2009). Cosmological perturbations of other interacting models have been investigated in Amendola et al. (2003); Koivisto (2005); Olivares et al. (2006); Mainini & Bonometto (2007); Bean et al. (2008); Vergani et al. (2009); Pettorino & Baccigalupi (2008); Schäfer (2008); Schaefer et al. (2008); La Vacca & Colombo (2008); He et al. (2009); Bean et al. (2008); Corasaniti (2008); Chongchitnan (2009); Jackson et al. (2009); Gavela et al. (2009); La Vacca et al. (2009); He et al. (2009); Caldera-Cabral et al. (2009); He et al. (2009); Koyama et al. (2009); Kristiansen et al. (2009).

2 PHENOMENOLOGY

We have performed 7 MCMC runs for the spatially flat ($\Omega = 1$) interacting model with various data sets (WMAP, WMAP&ACBAR, SN, BAO, WMAP&SN, WMAP&BAO, and WMAP&SN&BAO). Here WMAP refers to the 5-year temperature and polarization anisotropy data (Komatsu et al. 2009), ACBAR to the Arcminute Cosmology Bolometer Array Receiver data (Reichardt et al. 2009), SN to the Union Supernovae Ia sample (Kowalski et al. 2008) as implemented in CosmoMC[1] (Lewis & Bridle 2002, Lewis & Bridle) with systematic errors flag turned on, and BAO to the two data points $r_s(z_{\rm dec})/D_V(z=0.2)$ and $r_s(z_{\rm dec})/D_V(z=0.35)$ from Percival et al. (2007). For reference we have done also 6 MCMC runs (excluding WMAP&ACBAR from the above list) for the spatially flat non-interacting model. Each of these 13 runs has 3–4 chains with mean input multiplicity in the range 3–10, and the number of accepted models in each chain is ∼25000. The measure of mixing, the worst eigenvalue $R-1$ (which is better the closer it is to zero), is for all cases less than 0.03. More technical details are given in Appendix A.

Table A2 on page 14 in Appendix B collects the best-fitting models of each run (excluding WMAP&ACBAR). In addition, we show for each data-set two relatively good-fit models with a strong negative/positive interaction ($|\Gamma/H_0| > 0.1$) which are not 'far' from the best-fitting non-interacting model – in a sense that $\Delta\chi^2 = \chi^2$(strong interaction model) – χ^2(best-fitting model) < 4. In the last four rows of the table (Models 25–28) we show interacting models which have most of their parameters equal to the WMAP best-fitting non-interacting model (Model 1).

[1] http://cosmologist.info/cosmomc

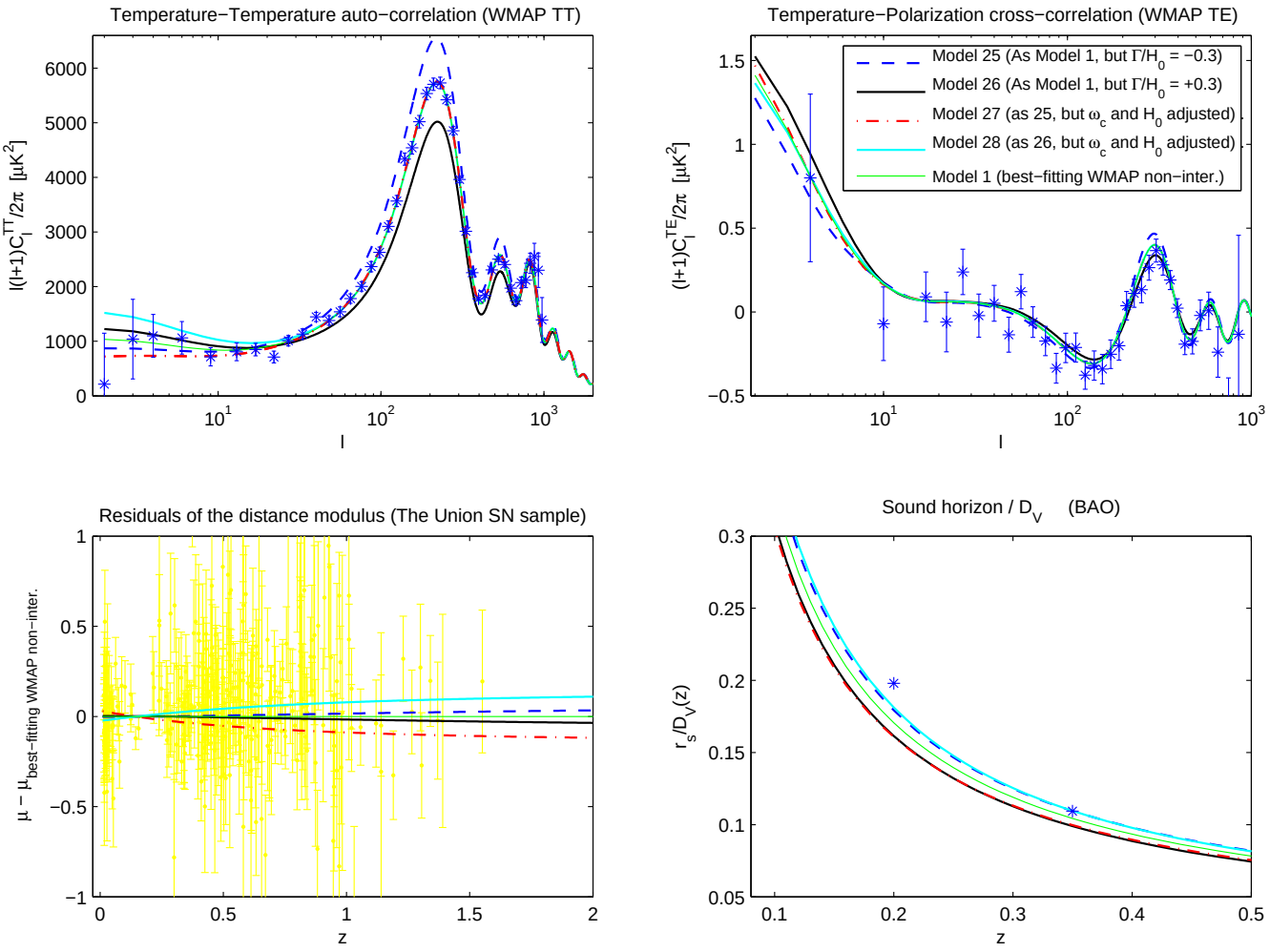

Figure 2. Models with most of their parameters equal to the parameters of the best-fitting to WMAP non-interacting model.

Fig. 2 shows the angular power spectra, distance modulus, and $r_s(z_{\rm dec})/D_V(z)$ for Models 25–28 and Model 1 from Table A2. The WMAP best-fitting non-interacting model (Model 1; thin green/grey line) fits well all the data. The only exceptions are that it fails to fit the low quadrupole $l = 2$ in the WMAP TT spectrum, and undershoots both the $z = 0.20$ and $z = 0.35$ BAO data points, whose error bars are smaller than the asterisk symbol in the plot. Therefore it would be surprising if the interacting model could fit the data overall much better. Now we take Model 1 and turn the interaction on to $|\Gamma/H_0| = 0.3$ (Models 25 and 26). The negative (positive) interaction leads to an extremely bad fit to the CMB TT data, as the the model now vastly overshoots (undershoots) the first and second acoustic peaks. This is also reflected in the TE spectrum where the peak at $l \sim 300$ is overshot (undershot). The SN data cannot distinguish the interacting model from the non-interacting model, though there is a tiny difference: a negative (positive) interaction leads to a faster (slower) increase of the distance modulus as a function of redshift than seen in the non-interacting model, and hence to a slightly better (worse) fit to the SN data. Finally, a negative interaction helps fitting the BAO data as it systematically shifts $r_s(z_{\rm dec})/D_V(z)$ upward. A positive interaction makes the fit to BAO data worse. All these remarks are reflected in the χ^2 values presented in Table A2.

It is quite straightforward to understand why a negative interaction helps in fitting the SN and BAO data. The negative interaction means that the energy transfer is from dark energy to dark matter. As we have kept today's values of ω_c (and Ω_{de0}) and H_0 fixed, this means that in the negatively interacting model there has been more dark energy in the past than in the non-interacting model. This causes more acceleration of the expansion of the universe, and hence larger distance moduli at high redshifts. In the BAO the distance measure is in the denominator, and at first sight one would expect smaller $r_s(z_{\rm dec})/D_V(z)$ than in the non-interacting case. However, as D_V is proportional to $D_A^{1/3}$ the effect of an increased angular diameter distance, $D_A(z)$, is mild. Instead the main effect now comes from the different sound horizon. For a fixed today's ω_c the negatively interacting model has a smaller cold dark matter density at last scattering $\omega_{\rm c}(z_*)$ than the non-interacting model. The sound horizon $r_s(z_{\rm dec})$ is proportional to $k_{\rm eq}^{-1}$ where $k_{\rm eq}$ is the wave number corresponding to the scale $\lambda_{\rm eq}$ that re-enters the horizon at matter-radiation equality. The smaller $\omega_c(z)$ at early times means that the matter density exceeds the radiation energy density later than in the non-interacting case.

As small scales re-enter the Hubble horizon before the large scales, $\lambda_{\rm eq}$ (or $k_{\rm eq}^{-1}$) and hence the sound horizon $r_s(z_{\rm dec})$ will be larger in the negatively interacting case. Table A2 confirms these conclusions (compare D_V and r_s in Models 1 and 25). The positive interaction model behaves vice versa.

Now we can explain also the bad fit to the CMB. The angular power spectrum is very sensitive to the dark matter density at last scattering $\omega_c(z_*)$ (or at the redshift of matter-radiation equality $z_{\rm eq}$). As the negative interaction model has a small $\omega_c(z_*)$ and hence a small $z_{\rm eq}$, the matter-radiation equality occurs very close to last scattering z_*. Therefore last scattering does not happen in the matter dominated era but around the transition from radiation domination to matter domination. This causes a large early integrated Sachs–Wolfe effect (eISW), which amplifies the first (and second) acoustic peaks. The angular power spectrum looks like that of a non-interacting model with a very small today's ω_c. The positive interaction model looks like a non-interacting model with a very high today's ω_c, i.e., the first and second acoustic peaks are vastly undershot (due to the early matter-radiation equality and hence a small eISW amplification). Therefore, in order to obtain a good fit to the CMB in the interacting model, we need to adjust today's ω_c in such a way that $\omega_c(z_*)$, or rather $a_{\rm eq}$, matches with the best-fitting non-interacting model. We have done this in Models 27 and 28; see Fig. 2 and Table A2. In the best-fitting non-interacting model (Model 1) today's dark matter density is $\omega_c = 0.107$, whereas to obtain a good fit with a negative (positive) interaction of $\Gamma/H_0 = -0.3$ $(+0.3)$ we require a larger $\omega_c = 0.137$ (smaller $\omega_c = 0.080$). As the larger (smaller) dark matter density leads to a smaller (larger) Ω_{de0}, the interacting model will now have a smaller (larger) angular diameter distance to last scattering $D_A(z_*)$. This would lead to all the acoustic peak structure shifting slightly to the left (right) from the WMAP data. As D_A is proportional to H_0^{-1}, this mismatch can be corrected by decreasing (increasing) the value of H_0 so that we obtain roughly the same $D_A(z_*)$ and hence the same acoustic peak positions as in the non-interacting case. With a negative (positive) interaction of $\Gamma/H_0 = -0.3$ $(+0.3)$, we require $H_0 = 56$ (66), while the best-fitting non-interacting model has $H_0 = 61\,{\rm km\,s^{-1}Mpc^{-1}}$. (Note: D_V and r_s in Table A2 are reported in units h^{-1}Mpc. The interacting Models 27 and 28 have $r_s = 154\,$Mpc, which is exactly the same as for the non-interacting Model 1.)

Fig. 2 and Table A2 show that after the above-described adjustments the strongly interacting $|\Gamma/H_0| = 0.3$ Models 27 and 28 provide an excellent fit to the CMB acoustic peaks. In the high-l ($l > 32$) region of the TT and all of the TE spectrum, the interacting models are totally indistinguishable from the non-interacting best-fitting Model 1. However, as the negatively interacting Model 27 has small $\Omega_{de0} = 0.49$ and hence also a smaller Ω_{de} in the recent past than the non-interacting model, the late integrated Sachs–Wolfe effect is suppressed, so there is less TT power at low multipoles. As the non-interacting model slightly over shoots the $C_l^{\rm TT}$ spectrum at low multipoles, the negatively interacting model leads to a better fit here; see Fig. 2 upper left panel and the column $\chi^{2\rm TT}_{l<32}$ in Table A2 for Models 1 and 27. (Note: the $\chi^{2\rm TT}_{l<32}$ numbers are from Gibbs sampling of the actual CMB map, and the more negative the number is the better the fit is.) The positive interaction Model 28 has a larger Ω_{de} in the recent times than the non-interacting model, and hence gives rise to a large late ISW effect, and a poor fit to low multipoles in the TT spectrum.

The SN data cover the relatively recent past only and hence the small $\Omega_{de0} = 0.49$ in the negative interaction Model 27 leads to a poorer fit. The SN data indeed slightly favour more acceleration in the recent past and the positive interaction Model 28 ($\Omega_{de0} = 0.76$) has this property, leading to a better fit to SN than the non-interacting Model 1, which has $\Omega_{de0} = 0.65$; see Fig. 2 lower left panel and the column $\chi^2_{\rm SN}$ in Table A2. For the same reason the negative interaction model fits the BAO data worse than the positive interaction model. Also the BAO data cover only the relatively recent past and favour more acceleration between redshifts $z = 0.20$ and $z = 0.35$ than the best-fitting non-interacting model provides.

Indeed already from Table A2 we can see these general trends. All the best-fitting interacting models (2, 14, 18, and 22) have negative Γ and are slightly better fits to the CMB due to sightly better fit to low-l CMB spectra. In general the best-fitting interacting models have indistinguishable $\chi^2_{\rm SN}$ and $\chi^2_{\rm BAO}$ from the best-fitting non-interacting models. The largest-$|\Gamma|$ models within $\Delta\chi^2 < 4$ from the best-fitting model (see Models 3, 4, 15, 16, 19, 20, 23, 24 in Table A2) always obey the following: a good-fit large negative interaction model is by about $\Delta\chi^2 = 1$–3 better fit to WMAP than a good-fit large positive interaction model, again due to the low-l behaviour. However, a negative interaction model is always a worse fit to both SN and BAO data (due to too small Ω_{de} in the recent past).

The ISW effect in the temperature angular power spectrum is given by

$$C_l^{ISW} = 4\pi \int_0^\infty \frac{k^3}{2\pi^2} \Bigg\{ \int_0^{\tau_0} \Big[\Big(\Psi'(\tau,k) - \Phi'(\tau,k) \Big) \times j_l\Big(k(\tau_0-\tau)\Big) e^{-\tau_{\rm od}(\tau,\tau_0)} \Big] d\tau \Bigg\}^2 \frac{dk}{k}\,, \qquad (6)$$

where j_l is the spherical Bessel function and $\tau_{\rm od}(\tau,\tau_0) = \int_\tau^{\tau_0} {\rm opacity}(\tilde\tau) d\tilde\tau$ is the optical depth from τ to today (τ_0). Note that at late times ($0 \leqslant z \lesssim 10$) we have $\Phi = -\Psi$, since the anisotropic stress vanishes. As it is the combination $\Psi' - \Phi'$ which defines the ISW effect, we show on the left panel of Fig. 3 the evolution of $\Psi - \Phi$ for the same models as in Fig. 2, i.e., Models 1 and 25–28 from Table A2. At high redshifts $z \gtrsim 10^4$, deep in the radiation era, the evolution in the interacting models is indistinguishable from the non-interacting model. If we keep all the other parameters fixed to the best-fitting non-interacting model, then a negative (positive) interaction leads to faster (slower) decay of the potential $\Psi - \Phi$ around the time of last scattering; compare the dashed blue (solid black) curves to the green curve on the left panel of Fig. 3. This matches to what we already explained about the early ISW effect: it is more (less) pronounced in the case of negative (positive) interaction, since the matter-radiation equality appears later (earlier) than in the non-interacting case. At late times, $0 \leqslant z \lesssim 10$, the interaction starts to modify the ISW source *directly*. The negative (positive) interaction leads to more gradual (steeper) decay of $\Psi - \Phi$, and to a smaller (an enhanced) late ISW effect.

If we adjust ω_c and H_0 (and hence Ω_{de0}) so that we ob-

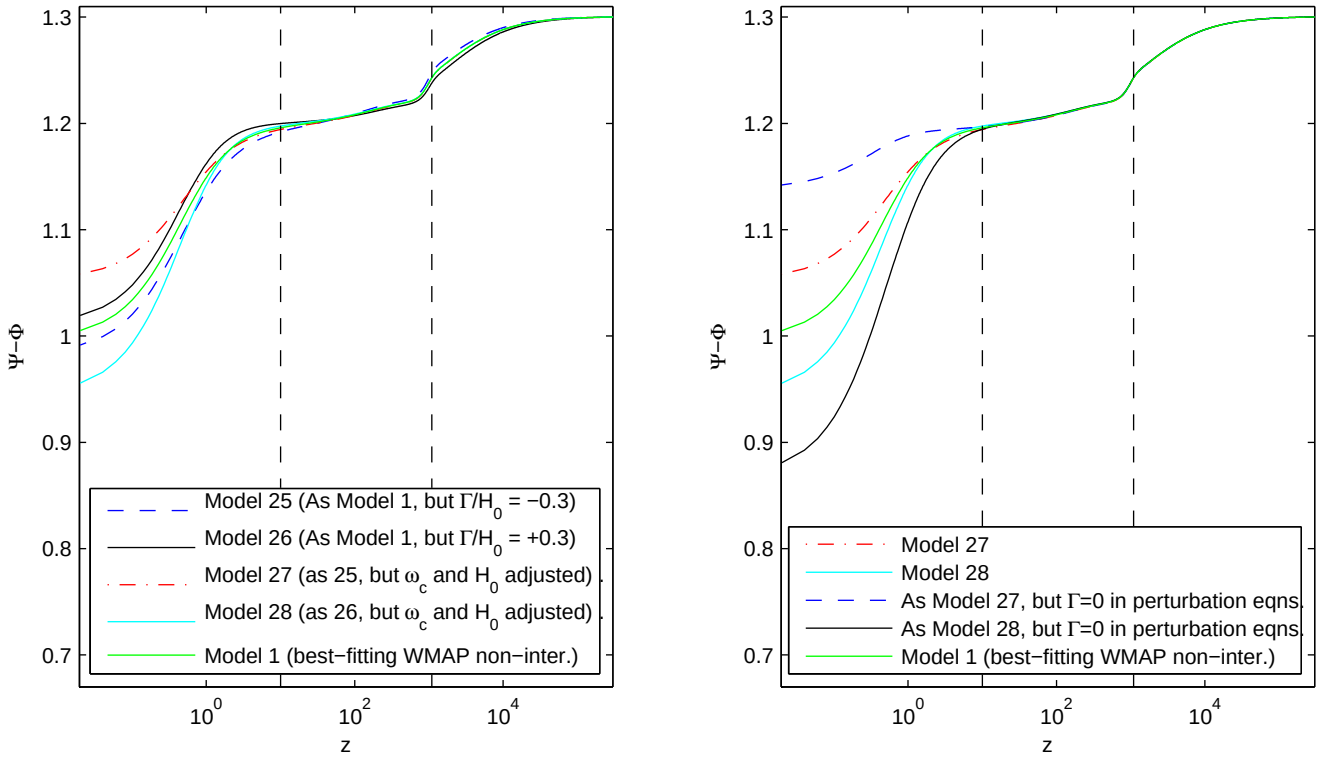

Figure 3. Redshift evolution of the ISW source. Dashed vertical lines indicate last scattering ($z \approx 1090$) and the time when the interaction starts to directly modify the evolution of the ISW source ($z \approx 10$).

tain the same $z_{\rm eq}$ as in the non-interacting case, and hence a perfect fit to the acoustic peaks in the data, the above-described effects on the late ISW effect become even more pronounced: compare the dot-dashed red (solid cyan) curves to the green curve on the left panel of Fig. 3. This is because with negative (positive) Γ we need a smaller (larger) Ω_{de0}, and so the background effect on the gravitational potential is to reduce (increase) its decay rate. Now an interesting question arises: how much of the late ISW effect in the good-fit models comes from the different background, i.e. different Ω_{de0} compared to the non-interacting best-fitting model, and how much comes from the modified perturbation evolution equations. The right panel of Fig. 3 addresses this question. Blue dashed (black solid) curves show how the negative interaction Model 27 (positive interaction Model 28) would behave if we ignored the interaction in the perturbation equations. Interestingly, we would drastically overestimate the effect of interaction on the late ISW effect. In the perturbation equations, see equations (11–14) or (29–41) in the companion paper (Majerotto, Valiviita & Maartens 2009), there seems to be a term which partially cancels the effect of different background evolution. This is easiest to see in the longitudinal (conformal Newtonian) gauge where $B = 0 = E$. As the dark energy perturbations remain subdominant, the interaction terms in their evolution equations cannot be responsible for the difference. Moreover, in the CDM velocity equation explicit interaction term is completely missing. So the only perturbation equation where the interaction appears to have an effect is the CDM density contrast equation, which in the longitudinal gauge reads

$$\delta_c' = 3\psi' - a\Gamma\phi\,. \qquad (7)$$

As long as the scale factor is small ($a \ll 1$) the evolution is like the non-interacting evolution, apart from the different evolution of the background, but in the later matter dominated era or dark energy dominated era, when a starts to approach 1, the interaction starts to modify directly the way the CDM reflects gravitational potential wells. In this era there is no anisotropic stress, so $\phi = \psi$, and let us assume that $\psi > 0$. Then due to the background effect of dark energy, $\psi' < 0$. Now the effect of the $-a\Gamma\phi$ term is that if $\Gamma < 0$ (> 0), then the CDM density contrast decays slower (faster) than in the non-interacting case. This in turn feeds back into the evolution of ψ via an Einstein equation (the general relativistic Poisson equation, equation (39) in the companion paper (Majerotto, Valiviita & Maartens 2009)). The effect is stronger the closer to 1 the scale factor is.

In the Newtonian gauge we can always neglect the dark energy perturbations, e.g. the total density contrast is $\delta = \delta\rho_c/\rho_{\rm tot}$ at late times. However, in synchronous gauge we cannot do this for the velocity perturbation since $\theta_c = 0$. Indeed, at late times $\theta_{\rm tot} \approx \theta_{de}$. But the second Einstein equation is $k^2\eta_s' = 4\pi G a^2(\rho + p)\theta_{\rm tot}$ – see e.g. equation (21b) in Ma & Bertschinger (1995) – and this is how the synchronous gauge metric perturbation η_s is calculated in CAMB (Lewis et al. 2000). So in synchronous gauge the interaction in the perturbation equations enters the ISW effect via the interaction in the θ_{de}' equation, (12) in the companion paper (Majerotto, Valiviita & Maartens 2009).

Note that it is difficult to go to very large positive in-

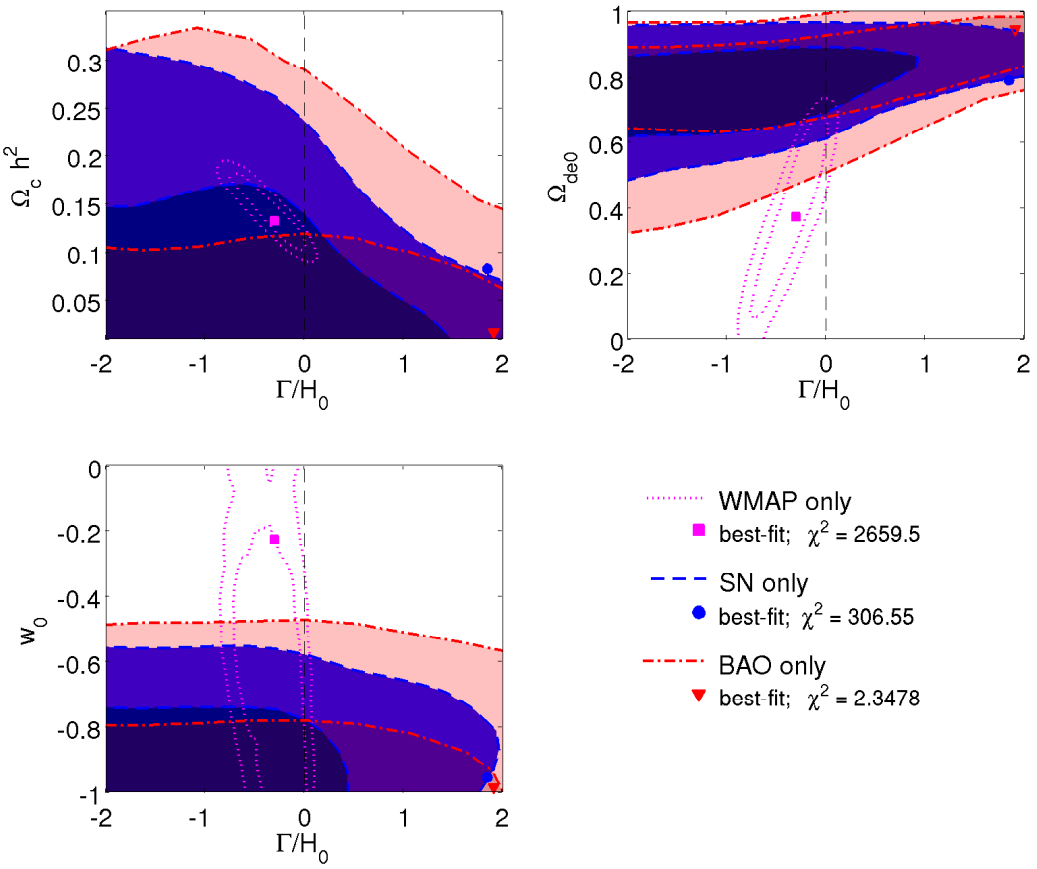

Figure 4. 2d marginalized likelihoods for the interacting model with only the WMAP, only the SN, and only the BAO data. The darker blue or red colours indicate 68% CL regions while the lighter blue or red colours indicate 95% CL regions with the SN or BAO data, respectively. The best-fits stand for the best-fitting models in the ranges shown in this figure. Therefore, here the BAO best-fitting model differs from the tabulated one which is at $\Gamma/H_0 = 2.92$; see Table A2.

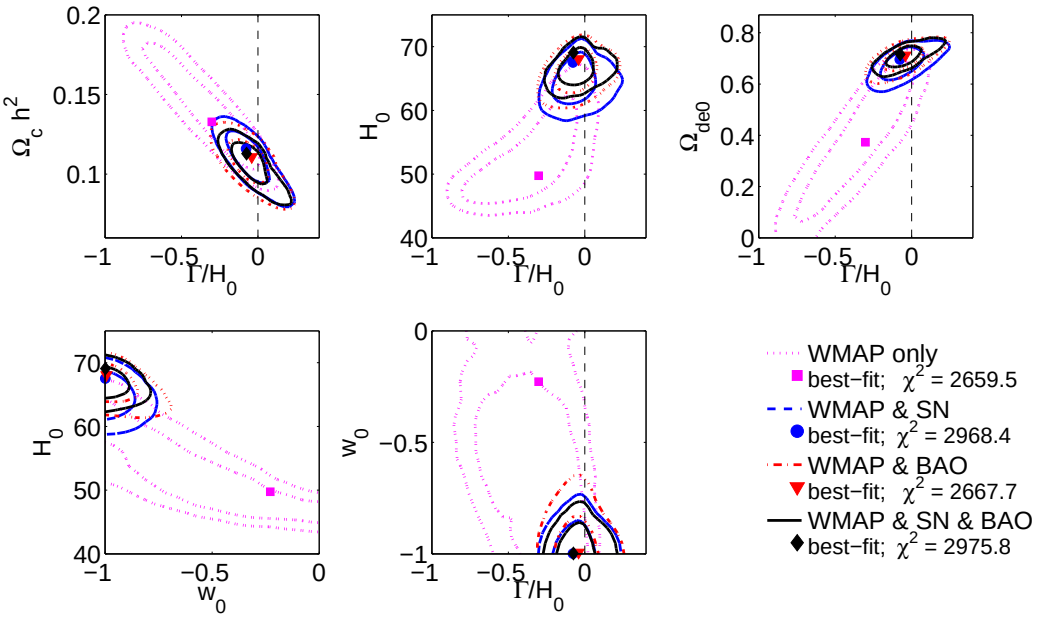

Figure 5. 2d marginalized likelihoods for the interacting model with the WMAP, WMAP&SN, WMAP&BAO and WMAP&SN&BAO data.

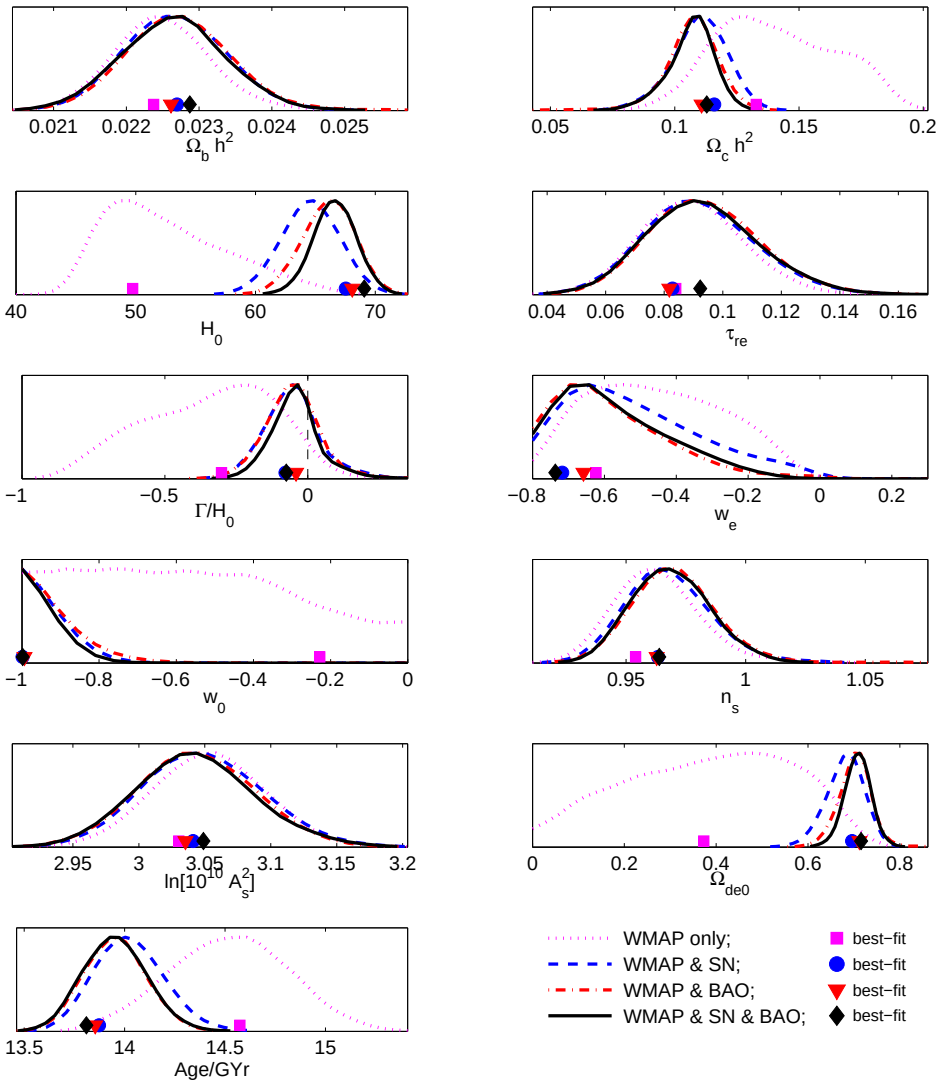

Figure 6. 1d marginalized likelihoods for the interacting model with the WMAP, WMAP&SN, WMAP&BAO and WMAP&SN&BAO data.

teractions, since the larger the Γ, the larger w_e one needs in order to avoid negative Ω_{de} in the past, i.e., to avoid the zero crossing of ρ_{de} which causes the perturbation equations becoming singular at that moment, as discussed in Appendix A3. So we expect the large interaction models to fit the CMB data as well as the non-interacting model, with negative Γ sightly favoured since this improves the fit in the low multipole region. Moreover, in marginalized likelihoods the negative interaction models will be favoured, since the ρ_{de} zero-crossing problem means that there is much less volume in the allowed parameter space in the positive Γ region than in the negative Γ region; see Appendix A3. There will be a strong degeneracy between ω_c and Γ, H_0 and Γ, and Ω_{de0} and Γ. When adding the other data (SN or BAO or SN&BAO) we expect most of the negative interaction models that fit the CMB alone well, to be excluded due to their very small Ω_{de} today and in the recent past.

3 LIKELIHOODS

As predicted, due to the degeneracy between ω_c and Γ/H_0, the CMB data alone do not provide tight constraints on the interaction. The degeneracy is almost linear, $\omega_c \simeq 0.107 - 0.1\,\Gamma/H_0$, according to Fig. 1, which shows 68% and 95% confidence level (CL) regions with WMAP, WMAP&ACBAR, and WMAP&SN&BAO data. As explained in the previous section, once ω_c (and H_0) are adjusted, the interacting model produces completely indistinguishable CMB angular power spectra at $l \gtrsim 32$. Therefore, combining WMAP (which reaches up to $l \sim 1000$) with ACBAR (which reaches $l \sim 2000$) does not help at all. Indeed, even with the forthcoming Planck data one will not be able to improve the constraints presented in Fig. 1, unless supplemented with some other non-CMB data. This is because the only signature from the interaction appears in the ISW region, and there the accuracy of CMB data is already now cosmic variance limited.

Furthermore, we see from Fig. 1 that according to the marginalized likelihoods with the CMB data, negative inter-

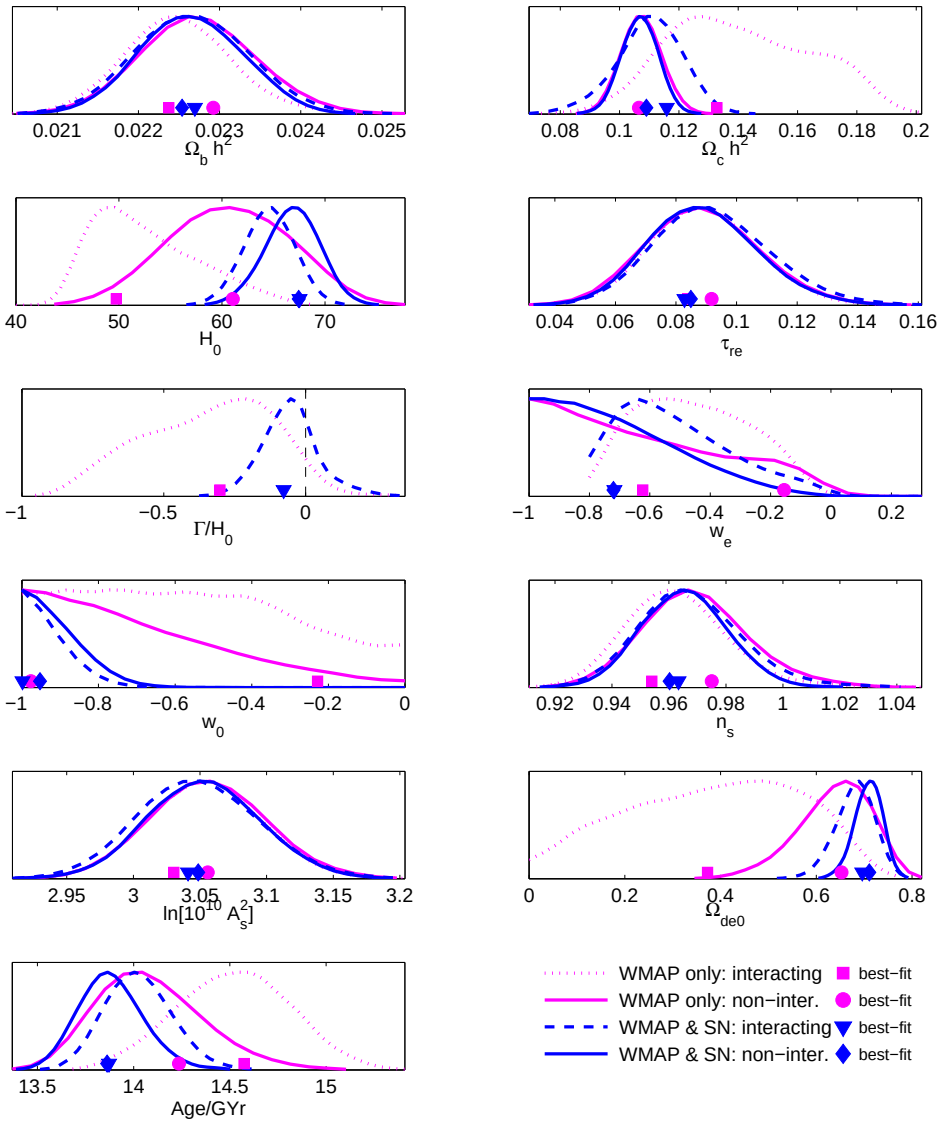

Figure 7. Comparison of 1d marginalized likelihoods for the interacting and non-interacting models with the WMAP and WMAP&SN data. The solid lines are for the non-interacting ($\Gamma = 0$) reference model.

actions are strongly "favoured" over positive interactions. As explained in Appendix A3, this is partially due to a volume effect caused by shrinking of the allowed w_e direction of parameter space for large positive interaction. In addition, positive interactions worsen the fit to the ISW region, while negative interactions improve it. According to Fig. 1, the 95% CL region of Γ/H_0 extends from -0.9 to +0.1. However, it should be noted that even stronger than -0.9 negative interactions would become allowed, if we lowered the lower bounds of two of our top-hat priors: $40 < H_0 < 100$, and $0 < \Omega_{de0} < 1$. This becomes evident later in the second and third panels of Fig. 5.

Adding SN and BAO data to the analysis leads to a more symmetric 95% CL region $-0.23 < \Gamma/H_0 < +0.15$, as seen in Fig. 1. In this case, the worse fit to ISW and the volume effect from w_e in the case of positive interaction become cancelled by better fits to the SN and BAO data. In order to gain more insight into this, in some cases dangerous, competition between the CMB and other data, we compare in Fig. 4 selected 2d marginalized posterior likelihoods when using only WMAP or only SN or only BAO data.

The SN or BAO data alone do not significantly constrain any parameters of our model other than those shown in Fig. 4, i.e., they push ω_c down to $\omega_c \lesssim 0.15$, Ω_{de0} up to $0.65 \lesssim \Omega_{de0} \lesssim 0.90$, and w_0 down to $w_0 \lesssim -0.75$ at 68% CL. The non-interacting model ($\Gamma = 0$) is consistent with all three data sets (WMAP, SN, BAO). Most interestingly, the non-interacting model sits in the intersection of all three data sets so that there is no tension between them. As already noticed, there is a tension between CMB and SN or CMB and BAO in the negatively interacting models. This tension is most pronounced in the top right panel (Γ, Ω_{de0}) of Fig. 4. However, the situation is not too bad since there is plenty of parameter space volume in the intersection of 95% CL regions of WMAP and SN or WMAP and BAO. Although the *SN or BAO data do not put any direct constraints on the interaction* (even $|\Gamma/H_0| \sim 3$ fits them well) the net effect of combining CMB with SN or BAO data is

to force $\Omega_{de0} \gtrsim 0.65$ and hence to cut away the large negative interaction models, leaving an almost symmetric region around $\Gamma = 0$. This effect is seen in the top left panel of Fig. 5, where we show 2d marginalized likelihoods from our MCMC runs for the interacting model with the WMAP data alone, the WMAP&SN, the WMAP&BAO, and the WMAP&SN&BAO data. The SN and BAO data are rather consistent with each other when constraining the interacting model. Therefore combining WMAP with either or both of them leads to very similar constraints, as seen in Fig. 5.

In Fig. 6 we show the 1d marginalized likelihoods for all of the primary MCMC parameters of our model and for two derived parameters: Ω_{de0} and the age of the universe. We note that WMAP combined with the BAO data prefers slightly larger today's Hubble parameter H_0 and dark energy density Ω_{de0} than with the SN data. The CMB data alone favour negative interactions and thus require small H_0 and Ω_{de0}. This corresponds to a very old universe as seen in the last panel of Fig. 6.

As mentioned above, from the 1d plot for Γ/H_0 in Fig. 6, the negative interaction seems more probable than the positive interaction. Indeed with the WMAP data (WMAP&SN&BAO data) 96.8% (77.6%) of models in our Markov Chains have a negative Γ, which means energy transfer from dark energy to dark matter. However, we should be cautious in claiming that the WMAP data (WMAP&SN&BAO data) favour energy transfer from dark energy to CDM at 96.8% CL (77.6% CL). It should again be stressed that this is partially the volume effect from the w_e direction of the parameter space. Indeed, recently Pereira & Jesus (2009) claimed that with 93% probability the data – which in Pereira & Jesus (2009) were the background-based data only – favour decay of dark matter to dark energy. Now we have about the same probability in favour of energy transfer from the dark energy to dark matter. The message here is that, in addition to the volume effect, these claims are highly model dependent: Pereira & Jesus (2009) studied an interaction proportional to ρ_{de} whereas our interaction is proportional to ρ_c.

We summarize here our most stringent results for the interacting model by giving minimal 95% intervals (Hamann et al. 2007) from our MCMC run with WMAP&SN&BAO data: $\omega_b \in (0.0212, 0.0241)$, $\omega_c \in (0.859, 0.125)$, $H_0 \in (63, 70)$, $\tau \in (0.057, 0.133)$, $\Gamma/H_0 \in (-0.23, +0.15)$, $w_e \in (-0.80, -0.19)$, $w_0 \in (-1.00, -0.63)$, $n_S \in (0.937, 1.002)$, $\ln(10^{10} A_S^2) \in (2.95, 3.14)$, $\Omega_{de0} \in (0.648, 0.767)$, Age$\in$ (13.6, 14.3) Gyr.

In Fig. 7 we compare the 1d marginalized likelihoods of the interacting model to the non-interacting reference model ($\Gamma = 0$). The key differences are: the interacting model leads to broader distributions of ω_c, H_0 and Ω_{de0}. This is due to the degeneracy between ω_c (or H_0 or Ω_{de0}) and Γ. Moreover, smaller H_0 is favoured by the interacting model. However, note again that this is partially a parameter space volume effect, since in our MCMC chains there are many more negative interaction models than positive interaction models, and the good-fit negative interaction models have small H_0. Finally we note that H_0, both in the interacting and non-interacting cases, is smaller than in the ΛCDM model, where a typical result of a likelihood scan peaks around $H_0 = 72\,\mathrm{km\,s^{-1}Mpc^{-1}}$. This is because we let w_0 (and w_a) vary, and there is a strong degeneracy (even in the non-interacting case) between H_0 and w_0 (or w_{de}). From Fig. 8 we see that a $w_0 = -1$ model prefers largest H_0 (and if we allowed $w_0 < -1$, even larger values of H_0 would be favoured).

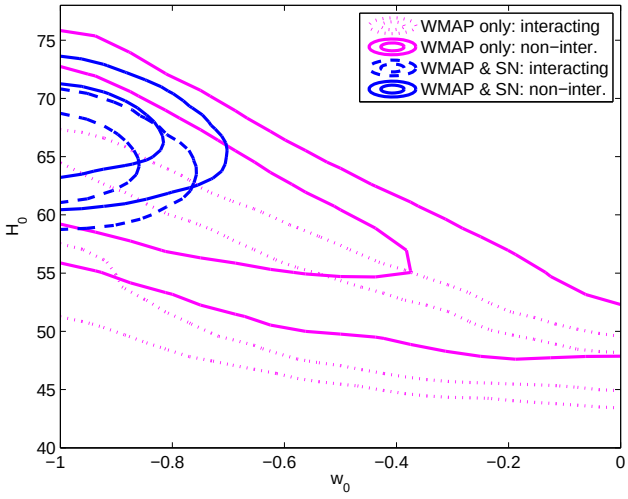

Figure 8. Comparison of a 2d marginalized likelihood for the interacting and non-interacting models with the WMAP and WMAP&SN data. Note the degeneracy between H_0 and w_0. The solid lines are for the non-interacting ($\Gamma = 0$) reference model.

4 ADDITIONAL CONSTRAINTS ON THE MODEL

In the two previous sections we have seen that any CMB data alone fail to constrain the interacting model, in particular with negative interaction, but the constraints from the SN or BAO data for the background dark energy density in the recent past cut out the strong interaction models with $\Gamma < 0$, as these models have very small Ω_{de}. In this section we briefly discuss some other data that could be used.

Most interestingly, as the interaction seems to affect the ISW effect only, accurate CMB – large-scale structure (LSS) cross-correlation data on the ISW effect (combined with other data sets such as CMB, SN and BAO) may turn out to set the most stringent constraints on the interaction. Firstly, the CMB–LSS cross–correlation data probe the evolution of Ω_{de} over time in the recent past. Secondly, as the interaction affects not only the background evolution, but directly the evolution of perturbations (in particular, the way that the evolution of the cold dark matter perturbation and gravitational potential are linked to each other) at redshifts probed by the ISW data, the ISW data may see the effects from the interaction most directly. We are working on this issue. While we were finalizing this paper, a work on other type of dark sector interaction appeared also suggesting that the interaction could be detected via its effects on the ISW signal (He et al. 2009). Earlier Lee et al. (2006) discussed the modified ISW effect in an interacting quintessence model. However, *they fixed all the other parameters* to (or near to) the best-fitting to WMAP Lambda CDM model. Therefore, although mentioning the degeneracy between Ω_{de0} (or ω_c) and the interaction rate elsewhere in their paper, they missed the degeneracy when finding con-

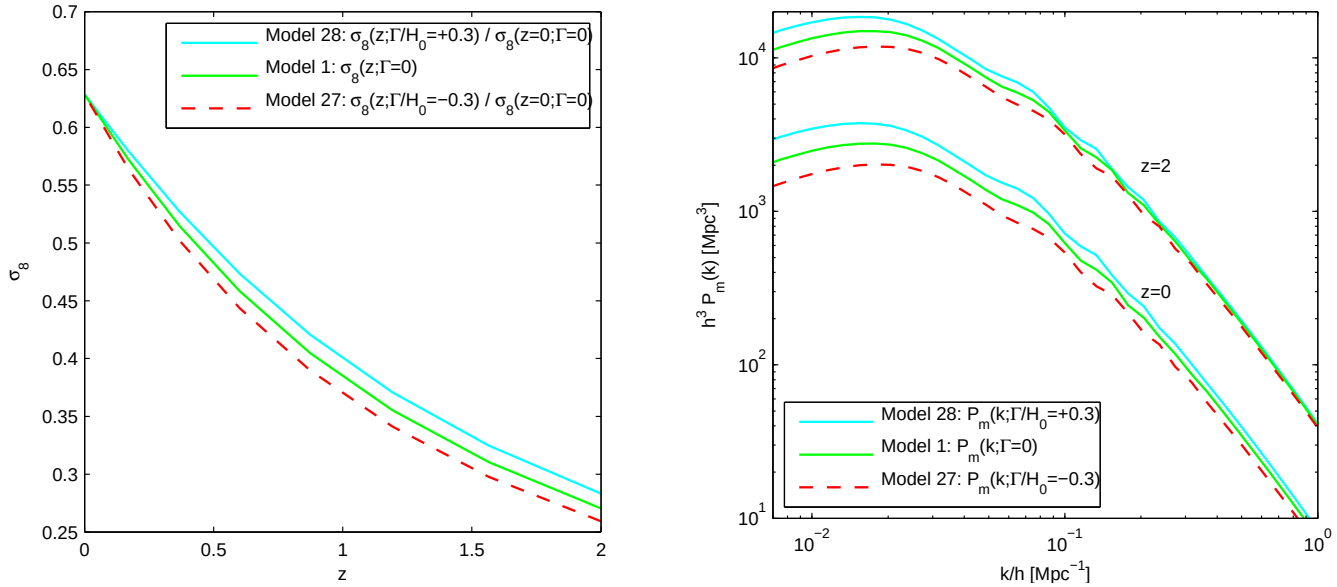

Figure 9. Redshift evolution of σ_8 and matter power spectrum.

straints on the interaction rate with WMAP data, ending up with artificially tight constraints on the interaction with CMB data alone. This can be seen, for example, in the third panel of our Fig. 5. Had we fixed Ω_{de0} to 0.76, as Lee et al. (2006) did, our constraint on the interaction rate would be misleadingly tight: $-0.03 \lesssim \Gamma/H_0 \lesssim +0.005$. It should be noted that although adding SN or BAO or SN&BAO into the analysis forces Ω_{de0} (and ω_c and H_0) closer to the best-fitting (to WMAP) Lambda CDM model and hence leads to a similar kind of effect as fixing the parameters, letting the other parameters freely vary and consequently *taking properly into account the degeneracy* gives much looser constraint: $-0.23 < \Gamma/H_0 < +0.15$ with WMAP&SN&BAO. So fixing the other parameters would misleadingly give more than an order of magnitude smaller 95% interval in our case.

Other interesting data come form the galaxy-galaxy power spectrum which is a probe of the underlying theoretical matter power spectrum. However, we have decided not to use these data here, since the exact relation between the observed galaxy-galaxy power spectrum and matter power spectrum is not known (due to redshift space distortions, non-linearities, etc) and moreover we calculate the perturbation evolution in the linear regime only. Probably the interaction would affect non-linear structure formation (Baldi et al. 2008; Baldi 2009). So at the moment it does not make sense to fit the shape of the (linear) matter power to the data. For similar reasons we do not consider weak-lensing data.

As the strongly interacting Models 27 and 28 in Table A2 have very different recent-time evolution of matter and dark energy densities, the overall amplitude of the matter power is affected. This results in different σ_8 (root mean square mass fluctuation on $8h^{-1}$ Mpc scale) than in the non-interacting model. We find that today $\sigma_8(z=0) = 0.598$, 0.628, 0.654 for Model 27 ($\Gamma/H_0 = -0.3$), Model 1 ($\Gamma = 0$), and Model 28 ($\Gamma/H_0 = +0.3$), respectively. Therefore, we predict that σ_8 measurements could rule out large negative interactions as they may lead to too small σ_8. On the left panel of Fig. 9 we show the redshift evolution of σ_8. We have normalized the curves for the interacting models to fit today's σ_8 of the non-interacting model. For example, for the $\Gamma/H_0 = -0.3$ model $\sigma_8(z=0)$ is smaller than in the non-interacting case, and towards the past it decreases even faster than in the non-interacting case. On the right panel of Fig. 9 we compare matter power spectra at redshifts $z = 0$ and $z = 2$ in the strongly interacting and non-interacting models. Small-scale (large k) shape is unaffected by the interaction, whereas large-scale (small k) shape (and amplitude) are affected significantly. Marginalizing analytically over the galaxy bias, the SDSS DR4 Luminous Red Galaxies sample (Tegmark et al. 2004, 2006) gives the best χ^2 for the positive interaction and worst χ^2 for the negative interaction, while the χ^2 of the non-interacting model falls between these two. As the effect of adding the LSS data to the analysis seems to be very similar to the effect of adding BAO or SN, we expect that adding the LSS data would give more weight to the positive interactions and hence lead to even more symmetric and tighter probability distribution about $\Gamma = 0$ than with the CMB&SN&BAO data.

5 CONCLUSION

In the companion paper (Majerotto, Valiviita & Maartens 2009) we have presented, for the first time, a *systematic* derivation of initial conditions for perturbations in interacting dark matter – dark energy fluid models deep in the radiation dominated era. These initial conditions are essential for studying the further evolution of perturbations up to today's observables. We have focused on the interaction $Q^\mu_c = -\Gamma\rho_c(1+\delta_c)u^\mu_c$, where Γ is a constant which has the same dimension as the Hubble parameter H; see Eqs. (1) and (2). In our previous work (Valiviita et al. 2008) we showed that if the equation of state parameter for dark energy is $-1 < w_{de} < -4/5$ in the radiation or matter dominated era, the model suffers from a serious non-adiabatic insta-

bility. However, in this paper (and in the companion paper (Majerotto, Valiviita & Maartens 2009)) we have shown that the instability can easily be avoided, if we allow for suitably time-varying dark energy equation of state. Our worked out example is for the parametrization $w_{de} = w_0 a + w_e(1-a)$. With this parametrization, viable cosmologies (in the interacting model) result whenever w_0 is close to -1 and $w_e < -1$ or $-4/5 \leqslant w_e \leqslant 1/3$, as long as $w_0 + 1$ and $w_e + 1$ have the same sign.

We have implemented into a publicly available Boltzmann integrator, CAMB, the background equations, and first order (linearized) perturbation equations, as well as the adiabatic initial conditions for the interacting model with time-varying equation of state parameter. We have performed full Monte Carlo Markov Chain likelihood scans for this model as well as for the non-interacting (Γ=0) model for a reference, with various combinations of publicly available data sets (WMAP, WMAP&ACBAR, SN, BAO, WMAP&SN, WMAP&BAO, WMAP&SN&BAO). To avoid ending up with too complicated shape of parameter space we have focused on non-phantom models, $-1 < w_{de} < 1/3$. (In addition, we consider phantom models to be unphysical.)

The main result is that there is a degeneracy between the interaction rate and today's dark energy (or dark matter) density in light of CMB data. Therefore, CMB data alone cannot rule out large interaction rates, not even Planck, since the high-multipole part of the CMB angular power spectra are totally indistinguishable from the non-interacting case. The only signal remaining from a large interaction rate would be a modified integrated Sachs-Wolfe effect, which makes using the ISW data an appealing line of future work. In this paper we have broken the degeneracy by Supernovae data and by baryon acoustic oscillation data, finding that the CMB&SN&BAO data constrain the interaction rate to about 20% of the expansion rate of the Universe.

Acknowledgments: JV and RM are supported by STFC. During this work JV received support also from the Academy of Finland. We thank Daniele Bertacca for comments, and acknowledge use of CosmoMC and CAMB. The MCMC analysis was mainly conducted in cooperation with SGI/Intel utilizing the Altix 3700 supercomputer at the UK-CCC facility COSMOS.

APPENDIX A: TECHNICAL DETAILS

A1 The code and modified sound horizon

We have modified publicly available CosmoMC (Lewis & Bridle 2002, Lewis & Bridle) and CAMB (Lewis et al. 2000) for this study. Into CAMB we have implemented the interacting evolution equations for the background (1) and (2), as well as the interacting perturbation evolution for dark energy, equations (11–14) from the companion paper (Majerotto, Valiviita & Maartens 2009), in the synchronous gauge: $B = \phi = 0$, $\psi = \eta_s$, and $E = -k^{-2}(6\eta_s + h_s)/2$, with η_s and h_s representing the synchronous gauge metric perturbations. In the synchronous gauge, the perturbed CDM equations of motion appear to look the same in the interacting and non-interacting cases, since $\phi = 0$. However, it should be noted that as the background evolves differently, it affects the evolution of h_s, and hence δ_c. We have implemented the initial conditions for perturbations deep in the radiation dominated era, specified in the companion paper (Majerotto, Valiviita & Maartens 2009).

In order to use the BAO data in the interacting model an additional modification to CAMB is necessary. In the standard version of CAMB/CosmoMC, the sound horizon is calculated by numerically integrating up to last scattering a_*

$$r_s(a_*) = \int_0^{\tau_*} c_s(\tau) d\tau = \int_0^{a_*} c_s(a)/a' da\,, \qquad \text{(A1)}$$

where c_s is the sound speed in the photon-baryon fluid and a_* is very accurately calculated from a fitting formula (Hu & Sugiyama 1996) which is valid if the matter scalings are the standard ones, $\rho_b \propto a^{-3}$ and $\rho_c \propto a^{-3}$. Firstly we need a different formula, as for BAO we want to integrate up to decoupling $a_{\rm dec}$, for which one has another fitting formula (Hu & Sugiyama 1996). Also this formula is valid only if $\rho_b \propto a^{-3}$ and $\rho_c \propto a^{-3}$. However, we know that this is not true for our case. Therefore we find $a_{\rm dec}$ numerically, and then calculate numerically

$$r_s(a_{\rm dec}) = \int_0^{a_{\rm dec}} c_s(a)/a'\, da\,. \qquad \text{(A2)}$$

The defining equation of decoupling is (Hu & Sugiyama 1996)

$$-\int_{\tau_0}^{\tilde\tau} R(\tau) \times \text{opacity}(\tau)\, d\tau = 1\,, \qquad \text{(A3)}$$

where $R = \frac{3}{4}\rho_b/\rho_\gamma$. We numerically follow this integral from today toward past times $\tilde\tau$ until the value 1 is reached. Then we record the value of the scale factor at this moment, name it $a_{\rm dec}$ and convert to a redshift $\tilde z_{\rm dec} = 1/a_{\rm dec} - 1$. Finally, to match the definitions in Eisenstein et al. (2007) and Percival et al. (2007) (from where we take the BAO data) we multiply the result by their "phenomenological" factor 0.96; $z_{\rm dec} = 0.96\tilde z_{\rm dec}$. We have verified that in the non-interacting case these definitions and our numerical routines lead to the same $z_{\rm dec}$ and $r_s(a_{\rm dec})$ as those given as a test case in Percival et al. (2007).

A2 The parameters and their prior ranges

In the interacting model we have 9 primary MCMC parameters which we vary over wide ranges with uniform (flat) prior over their range: the physical baryon density today $\omega_b = h^2\Omega_{b0}$, the physical cold dark matter density today $\omega_c = h^2\Omega_{c0}$, the Hubble parameter today H_0, optical depth to reionization τ_{re}, the interaction Γ in units of today's Hubble parameter, the early dark energy equation of state parameter w_e, the dark energy equation of state parameter today w_0, scalar spectral index n_S of the primordial perturbations, and the amplitude of primordial perturbations A_S [we use $\log_e(10^{10}A_S^2)$ as in the standard CosmoMC]. In the non-interacting reference model we have 8 free parameters as we keep Γ fixed to zero.

We exclude phantom models ($w_{de} < -1$) as unphysical, and we focus on the following ranges

$$-1 < w_0 < 0\,, \quad -1 < w_e < 0.3\,. \qquad \text{(A4)}$$

It should be noted that the CMB data actually exclude all

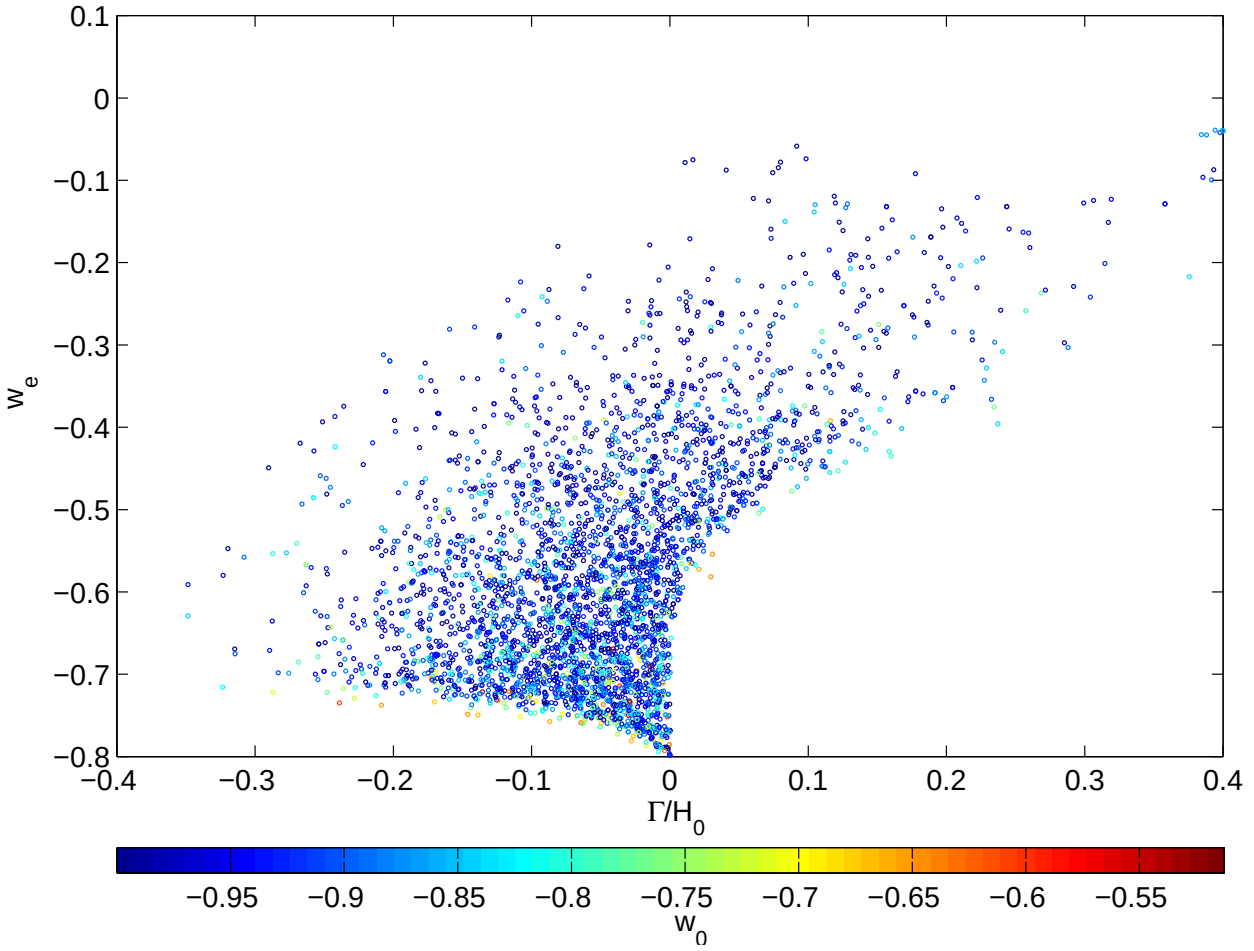

Figure A1. The w_e volume effect. The circles show samples from our MCMC run with the WMAP&BAO data. The colour scale indicates the value of w_0 for each sample.

blow-up models, i.e., the interacting models with $-1 < w_e < -0.8$. Keeping this in mind, our motivation to drop phantom models from the analysis becomes reinforced: it would make the posterior of w_e consist of two separate intervals, and hence the posterior likelihood of w_e would have two peaks, one with $w_e < -1$ and another one somewhere in the range $-4/5 \leqslant w_e < 1/3$. As the MCMC technique is particularly ill-suited for multiple peaked posteriors, allowing for phantom models would ruin the analysis. Moreover, we should demand $w_e + 1$ and $w_0 + 1$ to have the same sign, since otherwise there would be a time $\tau_{\rm oc}$ in the past where $w_{de}(a_{\rm oc}) = -1$. Such a 'minus one' crossing causes severe problems since the dark energy perturbation equations contain terms proportional to $1/(1 + w_{de})$, see the companion paper (Majerotto, Valiviita & Maartens 2009). The requirement $\mathrm{sign}(w_e + 1) = \mathrm{sign}(w_0 + 1)$ would further complicate the shape of the parameter space, if we allowed for $w_e < -1$ or $w_0 < -1$.

As discussed in Valiviita et al. (2008), $|\Gamma/H_0| \gg 1$ would conflict with the data. We find that a reasonable range is $\Gamma/H_0 \in (-4, +4)$. The ranges of other remaining primary MCMC parameters are: $\omega_b \in (0.005, 0.1)$, $\omega_c \in (0.01, 0.99)$, $H_0 \in (40, 100)$, $\tau \in (0.01, 0.4)$, $n_S \in (0.5, 1.5)$, $\ln(10^{10} A_S^2) \in (2.7, 4.0)$. Finally, we have an amplitude of the SZ template in CosmoMC, $A_{SZ} \in (0,\ 2)$, which is used when adding the SZ templates to the high-l part of the TT angular power spectrum. We also restrict the analysis to positive dark energy densities today, i.e., apply a top-hat prior $\Omega_{de0} > 0$. As we study spatially flat models, the matter density today is $\Omega_{m0} = 1 - \Omega_{de0}$.

In Table A1 we list some of the above-mentioned parameters as well as other symbols used in this paper.

A3 Positive Γ and zero-crossing of ρ_{de}

There is one additional complication in studying the interacting model and interpreting the marginalized posterior likelihoods. As pointed out in Valiviita et al. (2008), in the case of constant w_{de}, any *positive interaction* $\Gamma/H_0 > 0$ would lead to a zero crossing of ρ_{de}, or in other words Ω_{de}. This means that starting the background calculation from today's *positive* value, say $\Omega_{de0} \sim 0.7$, and integrating backward in time, at some moment $\tau_{de,\rm zc}$ in the the past $\Omega_{de}(\tau)$ crosses zero and becomes negative for $\tau < \tau_{de,\rm zc}$. While we lack deep understanding of the nature of dark energy we might even accept this possibility. However, the perturbation equations (11) and (12) in the companion paper (Majerotto, Valiviita & Maartens 2009), have the dark energy density in the denominator, and therefore become singular

symbol	explanation	defining equation / reference
subscript c	cold dark matter	
subscript de	dark energy	
subscript b	baryons	
subscript 0	variable evaluated today	
τ	conformal time	$d\tau = a^{-1}dt$, where a is the scale factor of the Universe
$'$	conformal time derivative	E.g. $a' = \frac{da}{d\tau}$
H	Hubble parameter, i.e., the expansion rate of the Universe	$H = \frac{da}{dt}/a$
$\mathcal{H}$	conformal Hubble parameter	$\mathcal{H} = a'/a = aH$
ω_b	physical density parameter of baryons	$\omega_b = \Omega_{b0}h^2$
ω_c	physical density parameter of cold dark matter	$\omega_c = \Omega_{c0}h^2$
$\rho_{\rm tot}$	total density	sum of energy densities of all constituents of the Univ.
n_S	scalar spectral index	
A_S	amplitude of the primordial curvature perturbation power	$\mathcal{P}_\mathcal{R}(k) = A_S(k/k_0)^{n_S-1}$, where $k_0 = 0.05$ Mpc^{-1}
τ_{re}	optical depth to reionization	
D_V	dilation scale	equation (2) of Eisenstein et al. (2005)
D_A	angular diameter distance	
$z_{\rm dec}$	redshift of decoupling	Eq. (A3) and explanation after that: $z_{\rm dec} = 0.96\tilde{z}_{\rm dec}$
z_*	redshift of last scattering	
r_s	sound horizon a decoupling	Eq. (A2)
ϕ, ψ, B, E	scalar metric perturbation variables	equation (6) of Majerotto et al. (2009)
Φ, Ψ	scalar gauge invariant metric perturbations	equations (6) and (25) of Majerotto et al. (2009)
η_s, h_s	synchronous gauge metric perturbations	these are called η and h in Ma & Bertschinger (1995)
θ_c	cold dark matter velocity perturbation	see e.g. (Valiviita et al. 2008; Ma & Bertschinger 1995)
θ_{de}	dark energy velocity perturbation	

Table A1. List of selected symbols used in this paper, with their physical meaning and defining equation or a reference.

at the moment $\tau_{de,\rm zc}$. For this reason, as discussed in Valiviita et al. (2008), all positive interactions with our type of interaction are ruled out if w_{de} is constant. However, the situation changes dramatically when we allow for time varying w_{de}. In viable models w_{de} today is close to -1 and then, as $-4/5 \leqslant w_e < 1/3$, going towards the past makes w_{de} less negative or even positive. If w_{de} becomes enough less negative *before* the moment $\tau_{de,\rm zc}$, then the zero crossing can actually be avoided. It turns out that the threshold value, $w_{e,\rm th}$, depends mildly on all the background density parameters and strongly on the interaction Γ/H_0 and, of course, w_0. The larger positive interaction we have, the larger w_e we need in order to avoid the zero-crossing of ρ_{de}, and hence the singularity of the perturbation equations. This means that for a given positive Γ (and the background parameters) all the models with $w_e < w_{e,\rm th}(\Gamma/H_0, w_0)$ will be missing from our Markov chains. There is no similar "top-hat cut-off" of models for negative Γ. This represents a difficulty in interpreting the marginalized posterior likelihoods. Let us assume a completely symmetric situation with respect to $\Gamma = 0$. Then without the cut-off, we would find 50% of the area under our 1d marginalized posterior for Γ/H_0 to lie in the negative Γ region, and 50% in the positive Γ region. However, with the cut-off unavoidably in operation, even if both positive and negative Γ models with $w_e > w_{e,\rm th}(|\Gamma|/H_0, w_0)$ led to exactly the same theoretical predictions (and hence to the same likelihoods), on the positive Γ side the marginalization integral over w_e collects only the volume $1/3 - w_{e,\rm th}(\Gamma/H_0, w_0) \ll 1.133$, while on the negative Γ side the volume factor is $1/3 - (-4/5) = 1.133$. The volume factor in the positive Γ side becomes smaller the larger Γ is. Therefore, even in this hypothetical "symmetric" situation, the marginalized likelihood for Γ would show a strong "preference" for a negative interaction.

We demonstrate the cut-off effect in Fig. A1, which shows samples from our Markov chains from the run with WMAP&BAO data. For example, if $\Gamma/H_0 = -0.1$, then the good-fit region is $-0.75 \lesssim w_e \lesssim -0.2$, whereas for $\Gamma/H_0 = +0.1$, all the models $-0.8 \lesssim w_e \lesssim -0.45$ are forbidden because of the zero crossing of ρ_{de}. Fig. A1 shows also that when w_e is very negative, we can to some extent compensate this with less negative w_0, as mentioned above.

With negative values of Γ we see in Fig. A1 another, milder, cut-off of models between $-4/5 < w_e < -2/3$. Asymptotically with large interactions this cut-off line approaches $w_e = -2/3$. From Table 1 on page 3 we can find an explanation for this behaviour. Although perturbations in the radiation era behave well and we can set adiabatic initial conditions, there is a rapidly growing non-adiabatic mode in the matter era, if $-4/5 < w_e < -2/3$. This mode kicks in faster the stronger the interaction is. In addition, this mode grows the faster the further away from $w_e = -2/3$ we are. Therefore, some models with small interaction rate and/or w_e close enough to $-2/3$ survive.

APPENDIX B: BEST-FITTING MODELS

We have collected in Table A2 χ^2s and parameters of the best-fitting models from our MCMC runs with various data sets (Models 1–24), as well as the example models discussed in Sec. 2 and Figs. 2, 3, and 9 (Models 25–28). It should be noted that Models 6 and 10 (with $w_e < -0.8$) would be excluded by the CMB data due to the blow-up of perturbations, but since the SN and BAO data probe background quantities only, these models fit them well. As the χ^2 is rather insensitive to w_e almost equally well-fitting models with $w_e > -0.8$ do exist in our chains.

Table A2. The χ^2s and parameters of the best-fitting model from each of our 6 MCMC runs for the non-interacting model ($\Gamma = 0$) and from our 6 MCMC runs for the interacting model ($\Gamma \neq 0$). The rows "neg. Γ" and "pos. Γ" show the models with largest $|\Gamma|$ (found in our MCMC chains) such that χ^2 is within 4 ($\sim 2\sigma$ if the likelihood was Gaussian) from the corresponding best-fitting model.

Model		Data	χ^2	$\chi^2_{\rm WMAP}$	$\chi^2_{l<32}$	$\chi^{2\rm TT}$	$\chi^{2\rm TT}_{l<32}$	$\chi^2_{\rm SN}$	$\chi^2_{\rm BAO}$
1	best $\Gamma=0$	WMAP	2660.4	2660.4	1221.5	1023.5	-11.3	311.4	22.5
2	best $\Gamma\neq0$	WMAP	2659.5	2659.5	1221.5	1022.8	-11.6	368.2	63.7
3	neg. Γ	WMAP	2662.6	2662.6	1222.0	1024.9	-11.1	389.4	81.8
4	pos. Γ	WMAP	2663.4	2663.4	1222.2	1024.9	-11.0	316.1	27.6
5	best $\Gamma=0$	SN	307.6	–	–	–	–	307.6	1260
6	best $\Gamma\neq0$	SN	306.5	–	–	–	–	306.5	146.7
9	best $\Gamma=0$	BAO	3.3	–	–	–	–	334.9	3.3
10	best $\Gamma\neq0$	BAO	2.1	–	–	–	–	363.7	2.1
13	best $\Gamma=0$	WMAP&SN	2968.7	2660.7	1222.2	1023.6	-10.5	308.2	7.8
14	best $\Gamma\neq0$	WMAP&SN	2968.4	2660.3	1221.0	1024.1	-11.9	308.1	7.8
15	neg. Γ	WMAP&SN	2972.1	2660.8	1222.2	1023.6	-11.9	311.3	15.4
16	pos. Γ	WMAP&SN	2971.9	2663.9	1222.6	1024.6	-10.6	308.0	13.3
17	best $\Gamma=0$	WMAP&BAO	2667.3	2660.6	1222.2	1023.1	-10.4	308.8	6.9
18	best $\Gamma\neq0$	WMAP&BAO	2667.7	2660.4	1221.3	1023.7	-11.5	308.1	7.3
19	neg. Γ	WMAP&BAO	2671.7	2661.4	1221.7	1024.2	-11.7	309.3	10.3
20	pos. Γ	WMAP&BAO	2671.7	2664.8	1224.8	1023.9	-7.7	308.3	7.0
21	best $\Gamma=0$	WMAP&SN&BAO	2975.7	2660.6	1221.8	1023.5	-10.7	308.3	7.0
22	best $\Gamma\neq0$	WMAP&SN&BAO	2975.8	2660.4	1220.9	1024.0	-11.7	308.3	7.1
23	neg. Γ	WMAP&SN&BAO	2979.3	2662.3	1220.7	1025.6	-12.1	308.7	8.2
24	pos. Γ	WMAP&SN&BAO	2979.6	2664.3	1222.7	1025.5	-9.9	308.0	7.3
	Other models appearing in the figures for phenomenological considerations								
25	As Model 1, but $\Gamma/H_0 = -0.3$			3680.0	1223.6	2026.8	-9.0	310.5	12.3
26	As Model 1, but $\Gamma/H_0 = +0.3$			3789.9	1224.5	2150.0	-8.8	312.7	40.3
27	As 25, but ω_c (Ω_{de0}) & H_0 adjusted			2661.2	1222.1	1023.8	-11.4	323.3	41.4
28	As 26, but ω_c (Ω_{de0}) & H_0 adjusted			2671.4	1233.0	1022.9	0.2	307.8	10.0

Table A2 – *continued* The cosmological parameters of the best-fitting models. Today's Hubble parameter H_0 is in units $\mathrm{km\,s^{-1}\,Mpc^{-1}}$, the age of the universe is given in Giga years, the distance measure D_V at redshifts $z = 0.20$ and $z = 0.35$ as well as the sound horizon at decoupling, r_s, are in units of $h^{-1}\,\mathrm{Mpc}$, where h is defined by $H_0 = h\,\mathrm{km\,s^{-1}\,Mpc^{-1}}$. Ampl. denotes the primordial perturbation amplitude, indeed $\ln(10^{10}A_S^2)$.

Model	ω_b	ω_c	H_0	τ_{re}	Γ/H_0	w_e	w_0	n_s	Ampl.	Ω_{de0}	Age	$D_V^{0.20}$	$D_V^{0.35}$	r_s	$z_{\rm dec}$
1	0.0229	0.107	61.1	0.09	0	-0.16	-0.98	0.975	3.06	0.65	14.2	552.3	902.9	94.2	1017
2	0.0224	0.133	49.7	0.08	-0.30	-0.62	-0.23	0.954	3.03	0.37	14.6	507.9	799.2	77.2	1017
3	0.0229	0.196	47.1	0.10	-0.90	-0.66	-0.19	0.971	3.06	0.01	14.7	500.6	780.9	73.2	1017
4	0.0233	0.091	58.7	0.09	0.12	-0.13	-0.81	0.996	3.04	0.67	14.4	544.4	884.4	91.2	1018
5	0.0757	0.013	68.8	0.08	0	0.30	-0.98	0.970	3.04	0.81	13.3	566.2	937.3	13.0	1130
6	0.0338	0.083	74.6	0.08	1.85	-0.84	-0.96	0.970	3.04	0.79	11.3	565.9	938.0	75.5	1050
9	0.0457	0.010	68.3	0.08	0	-0.94	-0.99	0.970	3.04	0.88	17.4	582.3	992.6	111.7	1050
10	0.0079	0.010	89.7	0.08	2.92	-0.87	-0.98	0.970	3.04	0.98	12.8	592.7	1025	116.0	989
13	0.0225	0.109	67.5	0.08	0	-0.72	-0.95	0.960	3.05	0.71	13.9	559.2	924.7	104.0	1017
14	0.0227	0.116	67.5	0.08	-0.08	-0.72	-1.00	0.963	3.04	0.70	13.9	560.4	927.3	104.3	1017
15	0.0223	0.133	62.4	0.09	-0.25	-0.61	-0.99	0.955	3.05	0.60	14.1	550.2	900.0	96.8	1017
16	0.0236	0.084	64.6	0.11	0.19	-0.06	-1.00	1.005	3.06	0.74	14.1	561.6	926.3	99.7	1019
17	0.0226	0.107	70.2	0.09	0	-0.78	-0.99	0.959	3.04	0.74	13.8	562.6	933.3	106.4	1017
18	0.0226	0.111	68.1	0.08	-0.04	-0.66	-0.99	0.963	3.04	0.71	13.9	561.5	930.0	105.4	1017
19	0.0220	0.125	64.1	0.09	-0.21	-0.70	-0.97	0.944	3.01	0.64	14.1	553.6	909.8	100.7	1015
20	0.0228	0.089	68.9	0.09	0.13	-0.40	-0.99	0.969	3.03	0.76	13.9	565.1	938.2	107.7	1017
21	0.0227	0.107	68.8	0.09	0	-0.68	-0.99	0.964	3.05	0.73	13.8	562.6	933.3	106.4	1017
22	0.0229	0.113	69.1	0.09	-0.07	-0.74	-1.00	0.964	3.05	0.72	13.8	562.6	933.4	107.1	1017
23	0.0223	0.120	65.9	0.09	-0.21	-0.71	-0.95	0.956	3.01	0.67	14.0	555.5	915.4	103.9	1016
24	0.0233	0.089	67.9	0.09	0.13	-0.34	-0.97	0.983	3.03	0.76	13.9	562.7	931.8	105.8	1018
	Other models appearing in the figures for phenomenological considerations														
25	0.0229	0.107	61.1	0.09	-0.30	-0.16	-0.98	0.975	3.06	0.65	14.6	552.9	905.6	99.1	1016
26	0.0229	0.107	61.1	0.09	0.30	-0.16	-0.98	0.975	3.06	0.65	13.9	551.6	900.0	89.1	1020
27	0.0229	0.137	56.1	0.09	-0.30	-0.16	-0.98	0.975	3.06	0.49	14.4	538.3	868.5	86.6	1017
28	0.0229	0.080	66.1	0.09	0.30	-0.16	-0.98	0.975	3.06	0.76	14.0	563.1	931.1	102.0	1017

REFERENCES

Amendola L., 1999, Phys. Rev., D60, 043501
Amendola L., Quercellini C., Tocchini-Valentini D., Pasqui A., 2003, Astrophys. J., 583, L53
Amendola L., Tocchini-Valentini D., 2002, Phys. Rev., D66, 043528
Baldi M., 2009, preprint (arXiv:0906.5353)
Baldi M., Pettorino V., Robbers G., Springel V., 2008, preprint (arXiv:0812.3901)
Bean R., Flanagan E. E., Laszlo I., Trodden M., 2008, Phys. Rev., D78, 123514
Bean R., Flanagan E. E., Trodden M., 2008, Phys. Rev., D78, 023009
Bertolami O., Gil Pedro F., Le Delliou M., 2007, Phys. Lett., B654, 165
Billyard A. P., Coley A. A., 2000, Phys. Rev., D61, 083503
Boehmer C. G., Caldera-Cabral G., Lazkoz R., Maartens R., 2008, Phys. Rev., D78, 023505
Caldera-Cabral G., Maartens R., Schaefer B. M., 2009, JCAP, 0907, 027
Caldera-Cabral G., Maartens R., Urena-Lopez L. A., 2009, Phys. Rev., D79, 063518
Caldwell R. R., Linder E. V., 2005, Phys. Rev. Lett., 95, 141301
Cen R., 2001, Astrophys. J. Lett., 546, 77
Chevallier M., Polarski D., 2001, Int. J. Mod. Phys., D10, 213
Chimento L. P., Jakubi A. S., Pavon D., Zimdahl W., 2003, Phys. Rev., D67, 083513
Chongchitnan S., 2009, Phys. Rev., D79, 043522
Corasaniti P. S., 2008, Phys. Rev., D78, 083538
Doran M., Muller C. M., Schafer G., Wetterich C., 2003, Phys. Rev., D68, 063505
Eisenstein D. J., et al., 2005, Astrophys. J., 633, 560
Eisenstein D. J., Seo H.-j., Sirko E., Spergel D., 2007, Astrophys. J., 664, 675
Farrar G. R., Peebles P. J. E., 2004, Astrophys. J., 604, 1
Gavela M. B., Hernández D., Lopez Honorez L., Mena O., Rigolin S., 2009, JCAP, 7, 34
Guo Z.-K., Ohta N., Tsujikawa S., 2007, Phys. Rev., D76, 023508
Hamann J., Hannestad S., Raffelt G. G., Wong Y. Y. Y., 2007, JCAP, 0708, 021
He J.-H., Wang B., 2008, JCAP, 0806, 010
He J.-H., Wang B., Abdalla E., 2009, Phys. Lett., B671, 139
He J.-H., Wang B., Jing Y. P., 2009, JCAP, 0907, 030
He J.-H., Wang B., Zhang P., 2009, preprint (arXiv:0906.0677)
Hu W., Sugiyama N., 1996, Astrophys. J., 471, 542
Jackson B. M., Taylor A., Berera A., 2009, Phys. Rev., D79, 043526
Koivisto T., 2005, Phys. Rev., D72, 043516
Komatsu E., et al., 2009, Astrophys. J. Suppl., 180, 330
Kowalski M., et al., 2008, Astrophys. J., 686, 749
Koyama K., Maartens R., Song Y.-S., 2009, preprint (arXiv:0907.2126)
Kristiansen J. R., La Vacca G., Colombo L. P. L., Mainini R., Bonometto S. A., 2009, preprint (arXiv:0902.2737)
La Vacca G., Colombo L. P. L., 2008, JCAP, 0804, 007
La Vacca G., Kristiansen J. R., Colombo L. P. L., Mainini R., Bonometto S. A., 2009, JCAP, 0904, 007
Lee S., Liu G.-C., Ng K.-W., 2006, Phys. Rev., D73, 083516
Lewis A., Bridle S., CosmoMC Notes, http://cosmologist.info/notes/cosmomc.ps.gz
Lewis A., Bridle S., 2002, Phys. Rev., D66, 103511
Lewis A., Challinor A., Lasenby A., 2000, Astrophys. J., 538, 473
Linder E. V., 2003, Phys. Rev. Lett., 90, 091301
Ma C.-P., Bertschinger E., 1995, Astrophys. J., 455, 7
Mainini R., Bonometto S., 2007, JCAP, 0706, 020
Majerotto E., Valiviita J., Maartens R., 2009, preprint (arXiv:0907.4981), accepted by MNRAS.
Malik K. A., Wands D., Ungarelli C., 2003, Phys. Rev., D67, 063516
Olivares G., Atrio-Barandela F., Pavon D., 2005, Phys. Rev., D71, 063523
Olivares G., Atrio-Barandela F., Pavon D., 2006, Phys. Rev., D74, 043521
Percival W. J., et al., 2007, Mon. Not. Roy. Astron. Soc., 381, 1053
Pereira S. H., Jesus J. F., 2009, Phys. Rev., D79, 043517
Pettorino V., Baccigalupi C., 2008, Phys. Rev., D77, 103003
Quartin M., Calvao M. O., Joras S. E., Reis R. R. R., Waga I., 2008, JCAP, 0805, 007
Quercellini C., Bruni M., Balbi A., Pietrobon D., 2008, Phys. Rev., D78, 063527
Reichardt C. L., et al., 2009, Astrophys. J., 694, 1200
Sadjadi H. M., Alimohammadi M., 2006, Phys. Rev., D74, 103007
Schaefer B. M., Caldera-Cabral G. A., Maartens R., 2008, preprint (arXiv:0803.2154)
Schäfer B. M., 2008, MNRAS, 388, 1403
Tegmark M., et al., 2004, Astrophys. J., 606, 702
Tegmark M., et al., 2006, Phys. Rev., D74, 123507
Turner M. S., 1983, Phys. Rev., D28, 1243
Valiviita J., Majerotto E., Maartens R., 2008, JCAP, 0807, 020
Vergani L., Colombo L. P. L., La Vacca G., Bonometto S. A., 2009, Astrophys. J., 697, 1946
Wetterich C., 1995, Astron. Astrophys., 301, 321
Zimdahl W., Pavon D., 2001, Phys. Lett., B521, 133